Rationalization of Au concentration and distribution in AuNi@Pt core-shell nanoparticles for oxygen reduction reaction

*Wei An [1,2] and Ping Liu[1]**

[1]Chemistry Department, Brookhaven National Laboratory, Upton, NY 11973, US

[2]College of Chemistry and Chemical Engineering, Shanghai University of Engineering Science, Shanghai 201620, China

KEYWORDS: Core shell nanoparticles, ORR, durability, AuNi alloy, Pt shell, DFT.

ABSTRACT.

Improving the activity and stability of Pt-based core-shell nanocatalysts for proton exchange membrane fuel cell (PEMFC), while lowering Pt loading, has been one of the big challenges in electrocatlysis. Here, using density functional theory (DFT) we report the effect of adding Au as the third element to enhance the durability and activity of Ni@Pt core-shell nanoparticles (NPs) during the oxygen reduction reaction (ORR). Our results show that the durability and activity of a Ni@Pt NP can be finely tuned by controlling Au concentration and distribution. For a NiAu@Pt NP, the durability can be greatly promoted by thermodynamically favorable segregation of Au to replace the Pt atoms at vertex, edge and (100) facets on the shell, which are known to contribute much less to ORR activity than (111) facets, while still keeping the ORR

activity on the active Pt(111) shell as high as that of Ni@Pt nanoparticle, which strongly depends on the direct interaction with Ni interlayer. Our results not only highlight the importance of interplay between surface strain on the shell and the interlayer-shell interaction in determining the durability and activity, but also provide the guidance on how to maximize the usage of Au to optimize the performance of core-shell (Pt) nanoparticles. Such understanding allows us to discover the novel NiAu@Pt nanocatalyst for the ORR.

1. INTRODUCTION

Core(non-Pt metals, M)-shell (Pt) nanoparticles (denoted as M@Pt NPs) have held special status of being either high-performance cathode[1,2] or anode[3,4] catalyst for fuel cells.[5-10,11-14] For the oxygen reduction reaction (ORR: $O_2 + 4H^+ + 4e^- \rightarrow 2H_2O$) at cathode of fuel cells, however, the reaction causes overpotentials and losses in fuel cell efficiency on conventional Pt catalyst. In addition, the high cost for precious Pt also hinders the practical application of fuel cells. The introduction of a secondary metal like Co, Ni, and Fe was found to not only reduce Pt loadings and therefore the cost, but also serve as an important ingredient to promote the catalytic activity.[15,16-20] In addition, adding Au as the third element to form alloy cores and enhance the ORR activity of AuM@Pt NPs was also observed.[21,22] The size and surface contraction[23-27], local structural flexibility,[25] as well as smooth surface morphology[28,29] were considered as the key factors for enhancing activity. Yet the durability still remains a challenge. In this regard, Au, which has much higher dissolution potential (1.50V) than Pt (1.18V),[30] has shown the significant potential by either forming bimetallic[31] or ternary alloys with Pt.[22,32] The increased durability of Pt shell was proposed to associate with the lowered surface energy via Au segregation or the hindered formation of sub-surface oxygen due to the presence of near-surface Au. However, the

details of how Au plays during the ORR are barely studied, which prevents the further development of PtAu-based catalysts.

In this contribution, we took NiAu@Pt NP as a case study to rationalize the concentration and distribution of Au in tuning the ORR durability and activity using density functional theory (DFT). Ni@Pt NPs stood out as an ORR catalyst,[16,17,33-35] being able to effectively reduce the cost due to the use of nonprecious metal and speed up the rate-determining protonation of O-containing species, e.g. O[36, 37,38] or OH[1,39,40], on pure Pt by introducing the surface contraction using Ni core. However, the catalyst lacks durability as Ni is leached out from the core under the potential cycling.[8] Here, we constructed core-shell NPs using NiAu alloy as the core and monolyer (ML) of Pt as the shell, aiming to meet three challenges by varying the concentration and distribution of Au: (1) increasing the durability of Pt on the shell under the ORR conditions; (2) tuning the binding properties of Pt on the (111)-shell and therefore at least maintaining the ORR activity of Ni@Pt; (3) lowering the additional cost by limiting the Au loading. Our study gained insight into the origin of Au in promoting the catalytic durability and activity of Ni@Pt NPs, highlighting the importance of interplay between surface strain on the shell and the interlayer-Pt shell interaction. In addition, it also provided guidance on how to maximize the usage of Au to optimize the ORR performance of core-shell (Pt). Such understanding eventually led to the discovery of novel NiAu@Pt NP catalyst, which adopted the optimal concentration and distribution of Au, being able to assure the high durability, but still allowing a high ORR activity.

2. COMPUTATIONAL SECTION

2.1 Computational methods.

All calculations were performed by using DFT as implemented in the Vienna ab-initio simulation package (VASP).[41,42] The spin-restricted GGA-PW91 functional,[43] a plane-wave basis set with an energy cutoff of 400 eV, and the projector augmented wave (PAW) method[44] were adopted. The NP was placed inside the (38×38×38 $Å^3$) cubic supercell whose size is large enough such that the separation between NP and its image in three direction is >15Å. The Brillouin zone of the supercell was sampled by Γ-point only. The conjugate gradient algorithm was used in optimization, allowing the convergence of 10^{-4} eV in total energy and 0.02 eV/Å in Hellmann-Feynman force on each atom. We also tested the effect of employing spin-polarized DFT. The results showed that the differences introduced by using spin-were small, which were in the order of ~0.02eV for dissolution potentials and ~0.07eV for O-binding energy (denoted as BE-O).

The relative stability of various core-shell NPs were expressed by electrochemical dissolution potential of surface alloys in acids following ref.[30] BE-O/OH on the (111) terrace of a NP was calculated.[36,45-48] BE-O was defined as BE-O= E(O/NP) – E(H_2O) + E(H_2) – E(NP) and BE-OH was defined as BE-OH= E(OH/NP) – E(H_2O) + ½E(H_2) – E(NP), where E represented the total energy of O/OH adsorbed NP, a water molecule in gas-phase, a hydrogen molecule in gas-phase and bare NP. To calculate BE-O, we chose one identical 3-fold hollow site (i.e., the most stable O-adsorption site), which located at the center of (111)-Pt shell. The adsorbed OH has a top configuration with O bound with Pt atom. The solvent effect on the ORR energetic is included by adding corrections of H_2O taken from Norskov et al.[36] No geometry constraints were applied during the optimization in order to explicitly capture the subtle size- and shape-effect of technical NP catalyst. It is worthy to stress that our NP model is in stark somewhat different from the previously employed 'slab'[1a] or 'geometry-frozen NP model[49], which reduces

the computing time, but is too simplified to capture the huge surface contraction introduced at nanoscale for particles. Using our NP model, we were able to describe the interplay between surface contraction and local structural flexibility in determining the ORR durability and activity of the NPs. [1b, 25] In agreement with the experimental observations, the activity is likely to converges to the bulk limit when the particle size is at least 4 or 5 nm.[26] Calculated results based on our model should reflect both ligand effects and strain effects. [24,50-52]

2.2 Core-shell NP model.

A 2.2nm sphere-like (SP) truncated octahedral $Ni_{96}Au_{105}@Pt_{204}$ core-shell NP model (total 405 atoms) was constructed. We note here that the ionic relaxations using DFT may not optimize the NP away from the original conformation which is here a bulk terminated structure;[53] however, the truncated octahedral shape and the bulk-like atomic array the Pt-based core-shell NPs have been reported experimentally, where our NP model is able to well describe the experimental observation.[2,45,54] The core corresponded to a Ni/Au atomic ratio of 0.48/0.52 which was based on the experiments.[55] $Ni_{201}@Pt_{204}$ and Pt_{405} NPs with the same size and shape of $Ni_{96}Au_{105}@Pt_{204}$, as well as Pt(111) were also included for comparison. Recent studies showed that such more realistic NP model was able to effectively capture the variation of activity and durability with size and shape.[7,23,25] Au as an alloying component has the strongest tendency toward surface segregation in vacuum and under the ORR conditions, [56,57,58] which is generally considered as an adverse factor for durability. In our DFT calculations, the cases without and with segregation of Au to the interlayer (IL) between core and shell and the shell were all taken into considerations. Accordingly, three NP models were constructed (Figure 1). The first corresponded to 1ML of Pt shell supported by the NiAu bulk-alloy core, $Ni_{96}Au_{105}@Pt_{204}$ (Figure 1a). The second was developed based on $Ni_{96}Au_{105}@Pt_{204}$ with consideration of Au

atoms segregating to the IL, $Ni_{79}@Ni_{17}Au_{105}@Pt_{204}$ (Figure 1b,c). Due to insufficient amount of Au in the model (105 atoms), the IL was only partially covered by Au, where the effects of both Au IL (Figure 1b) and Ni IL (Figure 1c) were considered. By further segregation of Au to the shell, a $Ni_{79}@Ni_{17}Pt_{105}@Au_{105}Pt_{99}$ NP was constructed (Figure 1d,e). Here the Au segregation was carried out by exchanging position with the nearby Pt in the shell. As a result, the core is still Ni_{79} as $Ni_{79}@Ni_{17}Au_{105}@Pt_{204}$, but the IL and the shell consisted of $Ni_{17}Pt_{105}$ and $Au_{105}Pt_{99}$, respectively. Again, the effects of both Pt IL (Figure 1d) and Ni IL (Figure 1e) were again considered. In our model, Au atoms were distributed in a symmetric way by occupying vertex and corner sites preferentially, followed by (100) and then (111) facets based on stability of the position (Figure S1) shown in previous studies.[59,60] In general, the more easily the Pt atom in the shell dissolute, the more energy gain is obtained when it is replaced by Au. Indeed, our calculations show that Au prefers to segregate to the shell (Figure 1d,e), rather than staying in the core as a NiAu alloy (Figure 1a) or in the IL (Figure 1b,c) by 0.12 eV/atom and 0.15 eV/atom, respectively. Such energetics-driven restructuring was also observed in experiment which showed more Au atoms were segregated to the top layers with an increasing annealing temperature in thermal treatments of $Au_{0.5}Pt_{0.5}$ nanoparticles.[61] We should also note that our 2.2nm NP model is still much smaller compared to experimental NPs (>5nm).

3. RESULTS AND DISCUSSION

3.1. $Ni_{96}Au_{105}@Pt_{204}$ NP

In the present study, the core-shell NPs consisting of 96 Ni atoms, 105 Au atoms and 204 Pt atoms in three different structures, $Ni_{96}Au_{105}@Pt_{204}$ (Figure 1a), $Ni_{79}@Ni_{17}Au_{105}@Pt_{204}$ (Figure 1b,c) and $Ni_{79}@Ni_{17}Pt_{105}@Au_{105}Pt_{99}$ (Figure 1d,e), were used as a model core-shell NP to

understand the effects of core, in particular to target the first two challenges on the durability and ORR activity of the Pt shell respectively.

Poor durability is one of the major drawbacks of the Pt-based NPs for practical application as ORR catalysts, because Pt-based NPs containing transition metals like Fe, Co, and Ni are facing dealloying or dissolution of reactive metals to the solution under potentials.[62-64] Recent studies observed the significant effect of Au in enhancing the durability. [31,32] Here we took a further step to investigate the possible influence of Au distribution on the durability of $Ni_{96}Au_{105}@Pt_{204}$ NP. In our study, the size and shape of NPs as well as the composition were kept the same and only the Au distribution was changed. Following the previous study,[22,30] the durability of the NP was scaled using dissolution potential of Pt shell, U. Figure 2 displayed the calculated dissolution potentials for various NPs with respect to Pt(111). One can see that Pt(111) shows the higher durability than all the NPs. Due to the size effect, the dissolution potential of pure Pt_{405} NP is lower than Pt(111) (U= -0.19 V) which can be further lowered by replacing the core Pt with Ni, and forming $Ni_{201}@Pt_{204}$ NP (U= -0.27 V) (Figure 2). When replacing the Ni core for the stoichiometric AuNi alloy, $Ni_{96}Au_{105}@Pt_{204}$ (Figure 1a) NP is able to increase U to -0.23 V. A decreasing in U to -0.33 V/Pt atom is obtained in the case that Au atoms segregate from the core to the IL and form $Ni_{79}@Ni_{17}Au_{105}@Pt_{204}$ (Figure 1b,c), while the dissolution potential is raised close to that of Pt(111) (U = -0.04 V) when Au segregates to the shell and forms $Ni_{79}@Ni_{17}Pt_{105}@Au_{105}Pt_{99}$ NP (Figure 1d,e). That is, the durability of NiAu@Pt NP can be promoted by distributing Au to the shell, which is a thermodynamically favorable process; in contrast, the presence of Au in the IL is energetically unfavored and should be avoided, which can destabilize and decrease the durability of NiAu@Pt NP.

Despite a large number of publications on the ORR in PEMFCs, the exact ORR mechanism remains unknown and the understanding the electrocatalysis of ORR on Pt and its alloys is still challenging to both experimental and theoretical studies.[1, 65] The complex kinetics for the ORR on Pt-based catalysts has been extensively studied.[2,24,36,45,66,67] Either BE-O[36, 37-39,68,69] or BE-OH[1,39,40,48] has been selected as a descriptor to capture the difference in the ORR activity from one system to the next, where BE-O and BE-OH well correlate with each other. When BE-O/OH is too strong, the protonation of O or OH is likely to be the rate-determining step (RDS), which determines the major cause for overpotential in experiment; whereas when BE-O/OH is too weak, the reaction can be hindered by the formation of OOH. This corresponds to the left and right leg of the 'volcano' plot, respectively. The strong O/OH-Pt(111) interaction can make the proton and electron transfer to *O or *OH very difficult, which is the major cause for high overpotential in the ORR and can also deteriorate NP's durability and block the active sites. A slightly weaker BE-O/OH than Pt(111) is required to promote the ORR activity but too weak BE-O/OH would switch the RDS from *OH formation or removal to *OOH formation according to the 'volcano' plot.[1,36,48] It was predicted that tuning the Pt sites with BE-O ~0.2 eV or BE-OH ~0.1 eV more weakly than Pt(111) likely led to the optimal ORR activity at the top of volcano.

According to our calculations, the correlation between BE-O and BE-OH on NPs observed for metal surfaces[1,36,39] is also valid for the interested NPs (Figure 3). Accordingly, both BE-O and BE-OH can be used to scale the ORR activity. Our calculations show that the Pt(111) shell for all NPs studied display to varied degree a weaker BE-O/OH than Pt(111). As shown in Figure 4, the formation of Pt_{405} NP (BE-O = 1.87 eV) is capable to weaken the O-Pt bond on Pt(111) (BE-O = 1.74 eV). The weakening can be significantly improved by replacing the core with Ni (BE-O = 2.54 eV for Ni_{201}@Pt_{204}). According to the volcano plot from previous studies,

[36, 37-39,68,69] the calculated BE-O weakening (0.8eV) on going from Pt(111) to Ni_{201}@Pt_{204} NPs seems over-weakening the O binding, which cannot explain the enhanced ORR activity observed experimentally for Ni@Pt NP.[19,70] The discrepancy seems associated with the difference of NP size. As noted in Section 2.2, our NP model (2.2nm in size) is much smaller than those used in experimental NPs (>5nm). On the basis our previous study,[25] we expect that the weakening in BE-O on a bigger Ni@Pt NP will be less severe and move closer to the top of volcano than that of Ni_{201}@Pt_{204} NP. Therefore a higher ORR activity than Pt can be observed. Calculations on much larger NPs indeed confirmed that the strain plays the dominant role on the ORR activities for the core/shell nanoparticles and suggested that the diameter of the core/shell nanoparticles should be larger than 7 nm to reach the peak of ORR activities.[71] Accordingly, it is expected that BE-O/OH based on our 2.2nam NP model should be shifted down in the volcano plot for comparison with experimental results using big NPs.

For NiAu@Pt NPs (a-e, Figure 1), the calculated BE-Os vary significantly depending on how Au distributes. $Ni_{96}Au_{105}$@Pt_{204} binds oxygen (BE-O = 1.89 eV) more strongly than that of Ni_{201}@Pt_{204}. In the case of Ni_{79}@$Ni_{17}Au_{105}$@$Pt_{204,}$ segregating Au to the IL generates the heterogeneity on the Pt shell. Two different kinds of Pt on the (111) facet, or Pt(111) shell in our notation, are formed depending on whether the interacted IL is Au (b, Figure 1b) or Ni (c, Figure 1c). One can see in Figure 4 that the BE-O for the Pt(111) shell interacted with Au IL is stronger (BE-O = 1.78 eV) than $Ni_{96}Au_{105}$@Pt_{204}, while for those interacted with Ni IL (Figure 1c), BE-O (BE-O = 2.55 eV) is close to that of Ni_{201}@Pt_{204}. Similar situation is also observed in the case that Au segregate to the shell, Ni_{79}@$Ni_{17}Pt_{105}$@$Au_{105}Pt_{99}$, which results in the Pt(111) shells interacted with Pt (Figure 1d) and Ni ILs (Figure 1e). Again, the Pt(111) shell interacted with Ni IL provides an oxygen binding (BE-O = 2.60 eV) as weak as that of Ni_{201}@Pt_{204}; while it is

increased (BE-O = 2.07 eV) with Pt as IL (Figure 4). In general, replacing Ni core for NiAu alloy is likely to increase the interaction of Pt(111) shell in Ni_{201}@Pt_{204} NP with the key intermediates, O or OH. The segregation of Au introduces heterogeneity in the Pt(111) shell, where two different ORR activities are observed on the same NiAu@Pt NP. Only the Pt(111) shell interacted with Ni IL can display similar BE-O and therefore the ORR activity as Ni_{201}@Pt_{204}; in contract those interacted with either Au or Pt IL bind the reaction intermediates more strongly. Such stronger O-Pt(111) shell interaction than Ni_{201}@Pt_{204} NP can affect the ORR activity in twofold: (1) strongly beneficial to the ORR when moving BE-O/OH closer to the top of volcano plot; (2) detrimental to the ORR in the case that the corresponding BE-O/OH is even further away from the optimal value than that of Ni_{201}@Pt_{204} NP.

To understand the trend in durability and BE-O/OH, we estimated the strain on the Pt(111) shell ($S_{Pt\text{-}Pt}$) of various NPs following our previous work (Figure 4),[25] and calculated the d-center (ε_d) for Pt on (111) shell of the NPs (Figure 5), which has been found to scale well with BE on metal surfaces.[72] By carefully analyzing the detailed local structures of NiAu@Pt NPs, we find that the degree of surface contraction on the shell and the shell-IL interaction play a key role in determining the durability and activity. In general, the more the surface is contracted, the lower the durability of corresponding Pt shell is (Figure 4), while the binding towards the reaction intermediates is rather complex. According to the previous studies on both metal surfaces[50] and Pd@Pt NPs,[25] a linear-like relationship between the surface strain and the BE was observed, where the origin was associated with the modification of Pt electronic structure due to the surface strain. For NiAu@Pt NPs, different behaviors were observed. One can see that with the same size (2.2 nm) and shape (sphere-like), both BE-O (Figure 4) and ε_d (Figure 5) correlate with $S_{Pt\text{-}Pt}$ via a step-like trend. A plateau is observed at the region with large $S_{Pt\text{-}Pt}$ (< -4.5%),

where BE-O and ε_d are insensitive to compressive strain; while for the region with small strain (> -4.5%), both decrease with the increasing S_{Pt-Pt} via a linear-like trend. Compared to Pt(111), the formation of Pt_{405} NP introduces a surface contraction (S_{Pt-Pt} = -3.6%) (Figure 4). According to our calculations, S_{Pt-Pt} can be effectively tuned by modifying the core. The S_{Pt-Pt} for Pt_{405} is increased by 67% by using Ni as core and forming Ni_{201}@Pt_{204} NP. As a result, the Pt(111) shell gets deactivated by shifting the Pt ε_d away from the Fermi Level from -2.47 eV to -3.09 eV (Figure 5), which leads to the decreasing in Pt shell-core interaction or dissolution potential and O-Pt interaction (Figure 4). Therefore, a lowered durability and an enhanced activity were observed experimentally under the ORR condition on going from Pt NP to Ni@Pt NP.[19,70] Adding the third metal Au effectively releases the overall surface contraction of Ni_{201}@Pt_{204} NP and therefore promotes the durability. Compared to Ni_{201}@Pt_{204} NP, the lattice constant of Ni core is enlarged by alloying with Au and forming $Ni_{0.48}Au_{0.52}$ bulk alloy, which leads to the decreasing of S_{Pt-Pt} from -6.0% to -3.9% (Figure 4). Consequently, ε_d of Pt(111) shell upshifts to -2.50 eV (Figure 5). Such shift in ε_d helps in increasing Pt-Pt, Pt-core as well as Pt-O interactions. Therefore, the durability of Ni_{201}@Pt_{204} NP is promoted (Figure 2), while the binding to oxygen is strengthened (Figure 4). We should also note that the dependence of the ORR activity on ε_d can be very complex for different metals ranging from Fe to Au.[73] However, the current study is only for one kind of metal, Pt. As shown in Figure 5, the shift in ε_d of (111)-Pt shell from Pt NP to Ni@Pt and various NiAu@Pt NPs is relatively small, which is within 1 eV. Therefore, a relatively direct relationship among ε_d, S_{Pt-Pt} and BE-O/OH can be obtained.

Controlling the segregation and therefore the distribution of Au can be also essential to tune the surface contraction of $Ni_{96}Au_{105}$@Pt_{204} NPs. When Au segregation is limited to the IL (Ni_{79}@$Ni_{17}Au_{105}$@Pt_{204}) the surface contraction of Pt shell of $Ni_{96}Au_{105}$@Pt_{204} can be released

($S_{Pt\text{-}Pt}$ = -3.4%) via directly interacting with the Au IL (Figure 1b), while it is increased to -4.4% via directly interacting with the Ni IL (Figure 1c). Accordingly, ε_d of Pt(111) shell is shifted up to -2.28 eV and stays as -2.97 eV, which close to that of Ni_{201}@Pt_{204} (Figure 5), respectively. In this way, two different ORR activities can be provided from a single NP. In term of durability, the presence of inert Au in the IL significantly decreases the stability of Pt shell and the durability of Ni_{79}@$Ni_{17}Au_{105}$@Pt_{204} NP is lower than that of $Ni_{96}Au_{105}$@Pt_{204}; in comparison the contribution from the Pt(111) shell interacted with Ni IL is less significant (Figure 2). Ni_{79}@$Ni_{17}Pt_{105}$@$Au_{105}Pt_{99}$ with Au segregation all the way to shell is thermodynamically more favorable than Ni_{79}@$Ni_{17}Au_{105}$@Pt_{204} and $Ni_{96}Au_{105}$@Pt_{204}. The core includes only Ni atoms, the IL is a mix of Ni and Pt facets and the shell includes a mix of Au and Pt terraces (Figure 1d,e). Again, depending on the interacted IL, Pt (Figure 1d) or Ni (Figure 1e), the contraction on Pt(111) shell can be -4.3% and -5.0%, and consequently the corresponding ε_d shifts to -2.66 eV and -3.13 eV, respectively (Figure 5); yet the calculated BE-O is either lower or similar to that of Ni_{201}@Pt_{204} NP (Figure 4). The presence of inert Au on the shell greatly raises the dissolution potential of Pt shell on Ni_{201}@Pt_{204} NP by 0.23 V (Figure 2), while the BE-O and therefore the high ORR activity can be kept at the same level by the-Pt(111) shell interacted with Ni layer (in Figure 4). Our results indicate that the IL can have pronounced impact on the local geometric structure and electronic structure of Pt(111) shell.

In general, compared to Pt(111), the compressed strain or the shortened Pt-Pt bond length on the (111) shell is likely to weaken intermediate-Pt shell interaction by shifting ε_d away from the Fermi level.[52,74] This is the case for the NPs with small contractions, including Pt_{405}, Ni_{79}@$Ni_{17}Au_{105}$@$Pt_{204\ (Au\ IL)}$, and Ni_{79}@$Ni_{17}Pt_{105}$@$Au_{105}Pt_{99\ (Pt\ IL)}$; in contrast, Ni_{201}@Pt_{204}, Ni_{79}@$Ni_{17}Au_{105}$@$Pt_{204\ (Ni\ IL)}$, and Ni_{79}@$Ni_{17}Pt_{105}$@$Au_{105}Pt_{99\ (Ni\ IL)}$ NPs are all supported by Ni

IL, which leads to a larger surface contraction and more importantly the small variation in ε_d and therefore BE-O with the decreasing $S_{Pt\text{-}Pt}$. Such insensitivity of ε_d and BE-O to the variation in $S_{Pt\text{-}Pt}$ is unique, which to our best knowledge, has not been observed before for core-shell NPs. The origin is not due to size and shape, which are kept same in our study. In addition, it does not seem to depend on the large surface contraction on the Pt(111) shell. Instead, we find that such behavior is associated with the tuning capability of the interacted Ni IL. Compared to Au, Pt or Pd ILs, Ni IL binds the Pt(111) shell and therefore, the electronic modification to the supported Pt the most strongly. The strain normal to (111) surface between Ni IL and Pt shell ($N_{Pt\text{-}Ni}$) varies with $S_{Pt\text{-}Pt}$ in the (111) shell. As shown in Figure S2, the more negative $S_{Pt\text{-}Pt}$ is, the more negative $N_{Pt\text{-}Ni}$ will be. That is, the strongly compressed Pt-Pt bond on the shell is accompanied with a strengthened Pt shell-Ni IL interaction along (111) direction. The former tends to destabilize Pt, while the latter increases the stability of Pt. With the decreasing in surface contraction, the normal strain is also released accordingly. The contribution from the two strains operating in an opposite way makes Pt ε_d stay at similar level in spite of variation in $S_{Pt\text{-}Pt}$. Our findings of insensitive ε_d and BE-O to $S_{Pt\text{-}Pt}$ due to the unique interaction between Pt shell and Ni IL can have significant impact on the development of ORR catalysts. It indicates that a good catalyst for ORR does not necessarily provide a moderate activity to compromise the high durability and high ORR activity.

According to the first two challenges we aim to meet for AuNi@Pt NPs, $Ni_{79}@Ni_{17}Pt_{105}@Au_{105}Pt_{99\ (Ni\ IL)}$ NP stands out, being able to promote the durability but maintaining the ORR activity of $Ni_{201}@Pt_{204}$ Au segregates to occupy the (100), edge and kink sites on the Pt shell, which are less stable and more prone to corrosion than the Pt(111) shell during the ORR. Such segregation not only stabilizes the entire NP, but also prevents the

dissolution of the Pt(111) shell. In term of ORR activity, due to the insufficient number of Au to cover the IL and the shell, the heterogeneity is introduced by Au segregation. It leads to the formation of Pt(111) shell supported by Ni IL, which displays similar to that of $Ni_{201}@Pt_{204}$ NP. The disadvantage for $Ni_{79}@Ni_{17}Pt_{105}@Au_{105}Pt_{99}$ NP is that due to the big loading of Au the third challenge of lowering additional cost cannot be met and the active Ni IL-supported Pt(111) shell is only 25% of the active (111)-facets. Therefore, theAuNi@Pt NPs with decreased amount of Au will be studied in the following.

3.2 $Ni_{96}@Au_xPt_{204-x}$

The results on NiAu@Pt NPs indicate three important factors to promote the durability and maintain the same ORR activity as Ni@Pt by adding Au. Firstly, the core should mostly consist of Ni, as only Ni IL-supported Pt(111) shell is able to keep the high ORR activity as Ni@Pt, while the presence of Au or Pt at the IL should be avoided. Secondly, the best way to increase the durability of Ni@Pt is that Au locates on the shell by replacing the Pt, in particular those at vertex and edge, which are less stable and more easily to dissolute than those on the terraces. Finally, the amount of Au at the shell should be limited to a certain extent, being large enough to replace Pt atoms on the shell that easily dissolute and therefore increase the catalyst durability, but small enough to keep the surface contraction large (< -4.5%) and maximize the amount of Pt(111) shell, which is active for the ORR. Following this idea, we varied the concentration of Au, aiming to target all three criteria, which is on durability, activity and cost respectively. Only the cases with decreasing amount of Au compared to $Ni_{96}Au_{105}@Pt_{204}$ were considered, as the increasing Au amount decreased the number of sites for the active Pt(111) shell supported by Ni

IL. In addition, the core was kept as pure Ni to assure the high ORR activity as Ni@Pt. Three model NPs were constructed based on the $Ni_{201}@Pt_{204}$ NP (Figure 6). That is, the size and shape are kept same as $Ni_{201}@Pt_{204}$ and $Ni_{96}Au_{105}@Pt_{204}$ NPs. The difference is the amount and position of the alloyed Au. The first is $Ni_{201}@Au_{108}Pt_{96}$ (Figure 6a), which has all (100) facets, edge and vertex sites are occupied by Au atoms similar to $Ni_{96}Au_{105}@Pt_{204}$, while the core is only consisted of Ni. Interestingly, we also observe a structural transformation of Au(100) facets to Au(111)-like facets (Figure 6a) during the geometry optimization. The second is $Ni_{201}@Au_{84}Pt_{120}$ (Figure 6b). The Au concentration decreases from 26.7% in the case of $Ni_{201}@Au_{108}Pt_{96}$ to 20.7%, where Au atoms only occupy the edge and vertex sites of $Ni_{201}@Pt_{204}$. The third is $Ni_{201}@Au_{24}Pt_{180}$ (Figure 6c). In this case, the amount of Au is further reduced to 5.9%, which uniquely only sit at the vertex sites of $Ni_{201}@Pt_{204}$. In addition, using these NP models allows us to understand the effect of lowering the Au amount on the durability and the ORR activity.

With the increasing Au amount, going from $Ni_{201}@Pt_{204}$, $Ni_{201}@Au_{24}Pt_{180}$, $Ni_{201}@Au_{84}Pt_{120}$ to $Ni_{201}@Au_{108}Pt_{96}$, the Pt atoms at vertex, edge and (100)-terrace sites of $Ni_{201}@Pt_{204}$ are replaced by Au sequentially (Figure 7). Due to the difference in stability of Pt at different positions (Figure S1), a big promotion in U is observed when the active vertex sites are occupied by Au, ($Ni_{201}@Au_{24}Pt_{180}$, Figure 7); in contrast the increase by occupying the edge sequentially is less significant ($Ni_{201}@Au_{84}Pt_{120}$, Figure 7). When further replacing the Pt(100) shell with Au ($Ni_{201}@Au_{108}Pt_{96}$, Figure 6a), U stays close to that of $Ni_{201}@Au_{84}Pt_{120}$, where the slight drop in U is associated with structural transformation of Au(100) to Au(111)-like shell (Figure 5a). A reverse trend is observed for BE-O/OH, which decreases with the increasing amount of Au on the shell (Figures 3, 4 and 7). In general, increasing Au concentration in the shell is able to

release the surface contraction from -6.0% for $Ni_{201}@Pt_{204}$ to -5.9% for $Ni_{201}@Au_{24}Pt_{180}$, -4.9% for $Ni_{201}@Au_{84}Pt_{120}$ and -4.8% for $Ni_{201}@Au_{108}Pt_{96}$ and therefore increase U; Yet, in comparison, as discussed in Section 3.1, the corresponding variation in ε_d and BE-O/OH is much less (Figures 3, 4 and 5). $Ni_{201}@Au_{84}Pt_{120}$ NP shows the highest durability among all the NPs studied, where U is close to that of Pt(111) (Figure 7). In term of activity, $Ni_{201}@Au_{24}Pt_{180}$ NP provides a BE-O/OH as weak as that of $Ni_{201}@Pt_{204}$; yet the BE-O/OHs for $Ni_{79}@Ni_{17}Au_{105}@Pt_{204\ (Ni\ IL)}$, $Ni_{79}@Ni_{17}Pt_{105}@Au_{105}Pt_{99\ (Ni\ IL)}$, and $Ni_{201}@Au_{84}Pt_{120}$ NPs are also close.

In consideration of the three challenges to target for AuNi@Pt NPs, we consider $Ni_{201}@Au_{84}Pt_{120}$ NP as the optimal. The first challenge is accomplished as among all NPs studied $Ni_{201}@Au_{84}Pt_{120}$ NP shows the highest durability. For the second challenge on the ORR activity, it maximizes the area of active Pt(111) shell as the case of $Ni_{201}@Pt_{204}$. In addition, the BE-O for the Pt(111) shell on $Ni_{201}@Au_{84}Pt_{120}$ NP is only 0.18 eV stronger than that of $Ni_{201}@Pt_{204}$ NP, which is very likely to locate in the optimal region of the volcano plot between BE-O and the ORR activity.[36,37] Finally, the Au loading is decreased to satisfy the third challenge of lowering the cost due to Au.

3.3 ORR on $Ni_{201}@Au_{84}Pt_{120}$ NP

In this section, we carried out mechanistic study of the ORR on $Ni_{201}@Au_{84}Pt_{120}$, making sure that the predicted ORR activity using BE-O/OH as a descriptor is valid. Pt(111) was also included for comparison. It's widely accepted that the ORR on Pt-based catalysts in acidic media proceeds via two reaction mechanisms:[36] (1) dissociative (direct) mechanism, in which O_2 is

directly reduced to H_2O: $O_2 + 4(H^+ + e^-) \rightarrow 2O^* + 4(H^+ + e^-) \rightarrow 2OH^* + 2(H^+ + e^-) \rightarrow 2H_2O$; (2) associative (indirect) mechanism, in which O_2 is indirectly reduced to H_2O through the formation of peroxy intermediate: $O_2 + 4(H^+ + e^-) \rightarrow OOH^* + 3(H^+ + e^-) \rightarrow O^* + OH^* + 3(H^+ + e^-) \rightarrow O^* + H_2O + 2(H^+ + e^-) \rightarrow OH^* + H_2O + (H^+ + e^-) \rightarrow 2H_2O$. One can be a dominant pathway over the other or they run in parallel depending on the working potential and the catalyst used.

We calculated the Gibbs reaction energy (ΔG) with salvation effect included along both pathways via both dissociative mechanism and associative mechanism using the model developed by Nørskov, et. al. [36] Accordingly, the reference potential setting was set to be that of the standard hydrogen electrode (SHE) and the chemical potential for the reaction ($H^+ + e^-$) was related to that of $1/2H_2$. It is important to stress that the above analysis on the ORR is the simplified without including the kinetic effects. However, for Pt and Pt alloys, extensive previous studies have shown that the difference in thermodynamics from one system to the next is able to capture that in the kinetics observed the experimentally.[1,36,37,40,75] The relative ORR activity our interest here and the accurate prediction is beyond the capability of current DFT.

As shown in Figure 8, our calculated energy diagrams for the ORR on Pt(111) agree well with the previous theoretical results for Pt(111) including the effect of water.[36] In general, all potential-dependent elementary steps less and less energetically favorable in both dissociative and associative mechanisms when increasing the potential (U) from 0 V to working potential (U=0.8V) and equilibrium potential (U= 1.23 V). In addition, following the same method, [36] we considered the most thermodynamically unfavorable step corresponding to the lowest abs(ΔG) as the most likely the RDS. At 0 V, the least exothermic step along the dissociative pathway and therefore the likely RDS is the first proton transfer or *O protonation, $^*O + H^+ + e^- \rightarrow {}^*OH$, along the dissociative pathway (ΔG= -0.78 eV); yet the second proton transfer, $^*OH + H^+ + e^- \rightarrow$

H_2O can also be important to the overall ORR with ΔG = -0.80 eV. At 0.8V, both *O and *OH protonation are thermonetrual (ΔG= 0.02 eV) and therefore the RDS, while the O_2 dissociation is highly exothermic. At 1.23 V, again *O (ΔG= 0.45 eV) and *OH (ΔG= 0.43 eV) protonation remain as the RDSs to slow down the reaction, while the endothermicity of the reaction increases. Along the associative pathway (Figure 8b), the first proton transfer or *O protonation to *OH is the least exothermic step at 0 V (ΔG= -0.52 eV). At 0.8V, both the proton transfer to *O is energetically unfavorable (ΔG= 0.28 eV) besides formation of *OOH via the O_2 protonation (ΔG= 0.26 eV). At 1.23 V, the *O protonation remains as the step with the highest endothermicity (ΔG= 0.72 eV). One can see that the likely RDS for the ORR on Pt(111) varies depending on the reaction mechanism and potentials. According the energetics, at the working potential of the ORR the proton transfer to adsorbed *O or *OH is likely to slow down the overall conversion, in agreement with the previous study.[36] Therefore, tuning the weakening the O/OH-Pt interaction has been predicted as an effective way to improve the ORR on Pt(111). We note here that the question about the real identity of the RDS in the ORR mechanism even on Pt(111) still remains open in both experiment and theory.[65] It has been claimed that the reduction of *OH or *O is the RDS of the ORR depending on the coverage of H_2O*, *O and *OH on the surface.[36,40,48,68,69] In this present work, we did not consider the effect of the surface species, but only including the corrections to the calculated BE in UHV condition at low coverage to describe the effect of water.[36] Nevertheless, the ORR on both NPs and Pt(111) is described under the same conditions for comparison, which is our interest here.

In comparison with Pt(111), $Ni_{201}@Au_{84}Pt_{120}$ NP behaves differently. As demonstrated above, the Pt(111) shell of the NP is less active than that on Pt(111). As a result, the reaction intermediates of the ORR on the NP is less stable than those on Pt(111) (Figure 8). At both U=

0V and U= 0.8 V (ΔG= 0.13 eV) along the dissociative pathway (Figure 8a), the potential-independent oxygen dissociation, $1/2O_2 \rightarrow O^*$, is the only thermoneutral step on the NP (ΔG= -0.06 eV), which is likely the least favorable step and therefore the RDS, while it is highly exothermic on Pt(111) (Figure 8a) and should proceed well under the ORR condition with a barrier of ~0.5 eV.[76] Yet, the overall ORR is downhill as the case of Pt(111). At U=1.23 V, the energetic preference for both *O and *OH protonation decreases close to thermoneutral, though the *OH protonation is slightly more energetically difficult than the rest steps. Along the associative pathway (Figure 8b), it's clear that the O_2 protonation to *OOH (ΔG= -0.65 eV at 0 V, 0.13 at 0.8 V, 0.55eV at 1.23 V) is critical for the ORR to proceed on the NP at all potentials; in contrast the other elementary steps are either more exothermic or less endothermic. In comparison with Pt(111), $Ni_{201}@Au_{84}Pt_{120}$ NP clearly behaves differently. Due to the weaker binding properties of Pt(111) shell of $Ni_{201}@Au_{84}Pt_{120}$ NP than Pt(111), strengthening the *OOH interaction becomes essential for facilitating the ORR at the working potential. By displaying a lower ΔG for the RDS than Pt(111) for the ORR via either dissociative or associative pathway, $Ni_{201}@Au_{84}Pt_{120}$ NP is likely to display a higher activity under realistic ORR potentials (0.8 V). That is, the ORR activity estimated using the BE-O/OH is valid. In this case, the potential hinders the protonation steps. As a result, on Pt(111) the rate-determining protonation of *O or *OH varies from thermodynamically favorable to unfavorable (Figure 8). On the NP the binding property of Pt(111) shell is deactivated selectively to *O rather than *OH, which promotes the exothermicity of the rate-determining protonation of *O to *OH. As a result, the corresponding ΔG stays negative at 0.8 V, which is more favorable than that on Pt(111) (Figure 8). Given that, the Pt(111) shell of $Ni_{201}@Au_{84}Pt_{120}$ NP is tuned to the optimal binding activities, being able to

catalyze both the O-O bind cleavage and the H-O bond formation better than Pt(111) under the ORR condition.

Finally, we note that the predictions from current theoretical work may also have impact on the practical applications. Firstly, we used a more realistic NP model, being able to well describe the difference from one system to the next in catalytic behaviors observed experimentally on technical powders.[22,45] In addition, the predicted structures of the NPs are thermodynamically stable, which can be possible to achieve by using fine-controlled synthesis method for practical applications.[21,75,77]

4. CONCLUSIONS

We employed DFT to investigate the effect of adding Au as the third element to the durability and activity of Ni@Pt core-shell NP during the ORR. According to our study, the catalytic property of Ni@Pt NP can be finely tuned by controlling the Au concentration and distribution. For a $Ni_{96}Au_{105}@Pt_{204}$ NP, the durability of Pt on the shell is greatly promoted by thermodynamically favorable Au segregation to replace the Pt atoms at vertex, edge and (100) facets on the shell ($Ni_{96}Au_{105}@Pt_{204} \rightarrow Ni_{79}@Ni_{17}Pt_{105}@Au_{105}Pt_{99}$), which are less stable and less active than those on (111) facets during the ORR. In contrast, the presence of Au in the interlayer is energetically unfavored and should be avoided, which destabilizes and decreases the durability of $Ni_{96}Au_{105}@Pt_{204}$ NP. The segregation of Au can also introduce heterogeneity in the Pt(111) shell of the NP. Depending on the species of the interacted interlayer, Ni or Pt(Au), two different ORR activities are observed on the same NP. Only the Pt(111) shell interacted with Ni interlayer can display similar ORR activity as $Ni_{201}@Pt_{204}$, while those interacted with either Au or Pt interlayer are less active.

On the basis of such understanding, we discovered $Ni_{201}@Au_{84}Pt_{120}$ NP as the best ORR catalysts, being able to fulfill the three challenges in durability, activity and cost. In this case the added Au atoms are designed to segregate to the shell and replace the vertex and edge Pt atoms. The concentration of Au is designed in a way, which is large enough to occupy all the vertex and edge sites on the shell, but small enough to keep the surface contraction large (< -4.5%) and maximize the area of Ni interlayer supported Pt(111) shell. In this way, $Ni_{201}@Au_{84}Pt_{120}$ NP displays the highest durability among all the NPs studied here, while the ORR activity is much higher than Pt and can be as promising as Ni@Pt NP. The Pt(111) shell of $Ni_{201}@Au_{84}Pt_{120}$ NP is tuned to the optimal binding activities, being able to catalyze both the O-O bind cleavage and the H-O bond formation better than Pt(111) under the ORR condition. Our study not only highlights the importance of interplay between surface strain on the shell and the interlayer-shell interaction in determining the durability and activity, but also opens new opportunity to optimize the performance of a core-shell NP towards the ORR by controlling the distribution and concentration of the components.

Supporting Information. Calculated Pt-5d projected density of states (PDOS) for a Pt shell atom at various sites of Ni and Ni@Pt NPs; variation in strain normal to (111) shell with that in (111) shell.

Corresponding Author

*Ping Liu, e-mail: pingliu3@bnl.gov.

ACKNOWLEDGMENT

The research was carried out at Brookhaven National Laboratory under contract DE-SC0012704 with the US Department of Energy, Division of Chemical Sciences. The DFT calculations were performed using computational resources at the Center for Functional Nanomaterials, a user facility at Brookhaven National Laboratory, and at the National Energy Research Scientific

Computing Center (NERSC), which is supported by the Office of Science of the U.S. DOE under Contract No. DE-AC02-05CH11231. The authors thank for the helpful discussion with Dr. Adzic at Brookhaven National Laboratory.

REFERENCES

(1) Stephens, I. E. L.; Bondarenko, A. S.; Gronbjerg, U.; Rossmeisl, J.; Chorkendorff, I. *Energy Environ. Sci.* **2012**, *5*, 6744-6762.

(2) Sasaki, K.; Naohara, H.; Choi, Y.; Cai, Y.; Chen, W.-F.; Liu, P.; Adzic, R. R. *Nat. Commun.* **2012**, *3*, 1115.

(3) Hsieh, Y. C.; Zhang, Y.; Su, D.; Volkov, V.; Si, R.; Wu, L. J.; Zhu, Y. M.; An, W.; Liu, P.; He, P.; Ye, S. Y.; Adzic, R. R.; Wang, J. X. *Nat. Commun.* **2013**, *4*, 2466.

(4) Alayoglu, S.; Nilekar, A. U.; Mavrikakis, M.; Eichhorn, B. *Nat. Mater.* **2008**, *7*, 333-338.

(5) Kleijn, S. E. F.; Lai, S. C. S.; Koper, M. T. M.; Unwin, P. R. *Angew. Chem., Int. Ed.* **2014**, *53*, 3558-3586.

(6) Schauermann, S.; Nilius, N.; Shaikhutdinov, S.; Freund, H. J. *Acc. Chem. Res.* **2013**, *46*, 1673-1681.

(7) Vines, F.; Gomes, J. R. B.; Illas, F. *Chem. Soc. Rev.* **2014**, *43*, 4922-4939.

(8) Somorjai, G. A.; Frei, H.; Park, J. Y. *J. Am. Chem. Soc.* **2009**, *131*, 16589-16605.

(9) Debe, M. K. *Nature* **2012**, *486*, 43-51.

(10) Jung, N.; Chung, D. Y.; Ryu, J.; Yoo, S. J.; Sung, Y. E. *Nano Today* **2014**, *9*, 433-456.

(11) Billinge, S. *Nature* **2013**, *495*, 453-454.

(12) Lim, B.; Jiang, M. J.; Camargo, P. H. C.; Cho, E. C.; Tao, J.; Lu, X. M.; Zhu, Y. M.; Xia, Y. N. *Science* **2009**, *324*, 1302-1305.

(13) Wang, D. L.; Xin, H. L. L.; Hovden, R.; Wang, H. S.; Yu, Y. C.; Muller, D. A.; DiSalvo, F. J.; Abruna, H. D. *Nat. Mater.* **2013**, *12*, 81-87.

(14) Lee, Y. W.; Ko, A. R.; Kim, D. Y.; Han, S. B.; Park, K. W. *RSC Adv.* **2012**, *2*, 1119-1125.

(15) Guo, S.; Zhang, S.; Sun, S. *Angew. Chem., Int. Ed.* **2013**, *52*, 8526-8544.

(16) Stamenkovic, V.; Mun, B. S.; Mayrhofer, K. J. J.; Ross, P. N.; Markovic, N. M.; Rossmeisl, J.; Greeley, J.; Norskov, J. K. *Angew. Chem., Int. Ed.***2006**, *45*, 2897-2901.

(17) Stamenkovic, V. R.; Mun, B. S.; Arenz, M.; Mayrhofer, K. J. J.; Lucas, C. A.; Wang, G. F.; Ross, P. N.; Markovic, N. M. *Nat. Mater.* **2007**, *6*, 241-247.

(18) Zhang, S.; Hao, Y. Z.; Su, D.; Doan-Nguyen, V. V. T.; Wu, Y. T.; Li, J.; Sun, S. H.; Murray, C. B. *J. Am. Chem. Soc.* **2014**, *136*, 15921-15924.

(19) Chen, Y. M.; Liang, Z. X.; Yang, F.; Liu, Y. W.; Chen, S. L. *J. Phys. Chem. C* **2011**, *115*, 24073-24079.

(20) Stamenkovic, V. R.; Mun, B. S.; Mayrhofer, K. J. J.; Ross, P. N.; Markovic, N. M. *J. Am. Chem. Soc.* **2006**, *128*, 8813-8819.

(21) Zhang, L.; Iyyamperumal, R.; Yancey, D. F.; Crooks, R. M.; Henkelman, G. *ACS Nano* **2013**, *7*, 9168-9172.

(22) Sasaki, K.; Naohara, H.; Cai, Y.; Choi, Y. M.; Liu, P.; Vukmirovic, M. B.; Wang, J. X.; Adzic, R. R. *Angew. Chem., Int. Ed.* **2010**, *49*, 8602-8607.

(23) Shao, M. H.; Odell, J. H.; Peles, A.; Su, D. *Chem. Commun.* **2014**, *50*, 2173-2176.

(24) Strasser, P.; Koh, S.; Anniyev, T.; Greeley, J.; More, K.; Yu, C.; Liu, Z.; Kaya, S.; Nordlund, D.; Ogasawara, H.; Toney, M. F.; Nilsson, A. *Nat. Chem.* **2010**, *2*, 454-460.

(25) An, W.; Liu, P. *J. Phys. Chem. C* **2013**, *117*, 16144-16149.

(26) Wang, C.; Chi, M.; Li, D.; Strmcnik, D.; van der Vliet, D.; Wang, G.; Komanicky, V.; Chang, K.-C.; Paulikas, A. P.; Tripkovic, D.; Pearson, J.; More, K. L.; Markovic, N. M.; Stamenkovic, V. R. *J. Am. Chem. Soc.* **2011**, *133*, 14396-14403.

(27) Jia, Q.; Caldwell, K.; Strickland, K.; Ziegelbauer, J. M.; Liu, Z.; Yu, Z.; Ramaker, D. E.; Mukerjee, S. *ACS Catal.* **2014**, *5*, 176-186.

(28) Cai, Y.; Ma, C.; Zhu, Y. M.; Wang, J. X.; Adzic, R. R. *Langmuir* **2011**, *27*, 8540-8547.

(29) Jung, N.; Chung, Y. H.; Chung, D. Y.; Choi, K. H.; Park, H. Y.; Ryu, J.; Lee, S. Y.; Kim, M.; Sung, Y. E.; Yoo, S. J. *Phys. Chem. Chem. Phys.* **2013**, *15*, 17079-17083.

(30) Greeley, J.; Norskov, J. K. *Electrochim. Acta* **2007**, *52*, 5829-5836.

(31) Zhang, J.; Sasaki, K.; Sutter, E.; Adzic, R. R. *Science* **2007**, *315*, 220-2.

(32) Wang, C.; van der Vliet, D.; More, K. L.; Zaluzec, N. J.; Peng, S.; Sun, S.; Daimon, H.; Wang, G.; Greeley, J.; Pearson, J.; Paulikas, A. P.; Karapetrov, G.; Strmcnik, D.; Markovic, N. M.; Stamenkovic, V. R. *Nano Lett.* **2010**, *11*, 919-926.

(33) Stamenkovic, V. R.; Fowler, B.; Mun, B. S.; Wang, G. F.; Ross, P. N.; Lucas, C. A.; Markovic, N. M. *Science* **2007**, *315*, 493-497.

(34) Cui, C. H.; Gan, L.; Heggen, M.; Rudi, S.; Strasser, P. *Nat. Mater.* **2013**, *12*, 765-771.

(35) Cui, C. H.; Gan, L.; Li, H. H.; Yu, S. H.; Heggen, M.; Strasser, P. *Nano Lett.* **2012**, *12*, 5885-5889.

(36) Norskov, J. K.; Rossmeisl, J.; Logadottir, A.; Lindqvist, L.; Kitchin, J. R.; Bligaard, T.; Jonsson, H. *J. Phys. Chem. B* **2004**, *108*, 17886-17892.

(37) Jackson, A.; Viswanathan, V.; Forman, A. J.; Larsen, A. H.; Nørskov, J. K.; Jaramillo, T. F. *ChemElectroChem* **2014**, *1*, 67-71.

(38) Yang, L.; Vukmirovic, M. B.; Su, D.; Sasaki, K.; Herron, J. A.; Mavrikakis, M.; Liao, S.; Adzic, R. R. *J. Phys. Chem. C* **2013**, *117*, 1748-1753.

(39) Rossmeisl, J.; Karlberg, G. S.; Jaramillo, T.; Norskov, J. K. *Faraday Discuss.* **2008**, *140*, 337-346.

(40) Hansen, H. A.; Viswanathan, V.; Nørskov, J. K. *J. Phys. Chem. C* **2014**, *118*, 6706-6718.

(41) Kresse, G.; Furthmuller, J. *Phys. Rev. B* **1996**, *54*, 11169-11186.

(42) Kresse, G.; Hafner, J. *Phys. Rev. B* **1993**, *47*, 558-561.

(43) Perdew, J. P.; Chevary, J. A.; Vosko, S. H.; Jackson, K. A.; Pederson, M. R.; Singh, D. J.; Fiolhais, C. *Phys. Rev. B* **1992**, *46*, 6671-6687.

(44) Blochl, P. E. *Phys. Rev. B* **1994**, *50*, 17953-17979.

(45) Wang, J. X.; Inada, H.; Wu, L. J.; Zhu, Y. M.; Choi, Y. M.; Liu, P.; Zhou, W. P.; Adzic, R. R. *J. Am. Chem. Soc.* **2009**, *131*, 17298-17302.

(46) Zhang, J.; Yang, H. Z.; Fang, J. Y.; Zou, S. Z. *Nano Lett.* **2010**, *10*, 638-644.

(47) Viswanathan, V.; Hansen, H. A.; Rossmeisl, J.; Norskov, J. K. *J. Phys. Chem. Lett.* **2012**, *3*, 2948-2951.

(48) Viswanathan, V.; Hansen, H. A.; Rossmeisl, J.; Norskov, J. K. *ACS Catal.* **2012**, *2*, 1654-1660.

(49) Li, L.; Larsen, A. H.; Romero, N. A.; Morozov, V. A.; Glinsvad, C.; Abild-Pedersen, F.; Greeley, J.; Jacobsen, K. W.; Nørskov, J. K. *J. Phys.Chem. Lett.* **2012**, *4*, 222-226.

(50) Kitchin, J. R.; Norskov, J. K.; Barteau, M. A.; Chen, J. G. *Phys. Rev. Lett.* **2004**, *93*.

(51) Kitchin, J. R.; Norskov, J. K.; Barteau, M. A.; Chen, J. G. *J. Chem. Phys.* **2004**, *120*, 10240-10246.

(52) Mavrikakis, M.; Hammer, B.; Norskov, J. K. *Phys. Rev. Lett.* **1998**, *81*, 2819-2822.

(53) Ferrando, R.; Jellinek, J.; Johnston, R. L. *Chem. Rev.* **2008**, *108*, 845-910.

(54) Hsieh, Y.-C.; Zhang, Y.; Su, D.; Volkov, V.; Si, R.; Wu, L.; Zhu, Y.; An, W.; Liu, P.; He, P.; Ye, S.; Adzic, R. R.; Wang, J. X. *Nat. Commun.* **2013**, *4*.

(55) Zhou, S. H.; Yin, H. F.; Schwartz, V.; Wu, Z. L.; Mullins, D.; Eichhorn, B.; Overbury, S. H.; Dai, S. *Chemphyschem* **2008**, *9*, 2475-2479.

(56) Ruban, A. V.; Skriver, H. L.; Norskov, J. K. *Phys. Rev. B* **1999**, *59*, 15990-16000.

(57) Herron, J. A.; Mavrikakis, M. *Catal. Commun.* **2014**, *52*, 65-71.

(58) Wang, J.; Zhang, Q.; Wang, Y. *Catal. Today* **2011**, *171*, 257-265.

(59) Zhang, Y.; Hsieh, Y. C.; Volkov, V.; Su, D.; An, W.; Si, R.; Zhu, Y. M.; Liu, P.; Wang, J. X.; Adzic, R. R. *ACS Catal.* **2014**, *4*, 738-742.

(60) Carino, E. V.; Kim, H. Y.; Henkelman, G.; Crooks, R. M. *J. . Am. Chem. Soc.* **2012**, *134*, 4153-4162.

(61) Suntivich, J.; Xu, Z. C.; Carlton, C. E.; Kim, J.; Han, B. H.; Lee, S. W.; Bonnet, N.; Marzari, N.; Allard, L. F.; Gasteiger, H. A.; Hamad-Schifferli, K.; Shao-Horn, Y. *J. Am. Chem. Soc.* **2013**, *135*, 7985-7991.

(62) Renner, F. U.; Stierle, A.; Dosch, H.; Kolb, D. M.; Lee, T. L.; Zegenhagen, J. *Nature* **2006**, *439*, 707-710.

(63) Erlebacher, J.; Aziz, M. J.; Karma, A.; Dimitrov, N.; Sieradzki, K. *Nature* **2001**, *410*, 450-453.

(64) Sieradzki, K.; Dimitrov, N.; Movrin, D.; McCall, C.; Vasiljevic, N.; Erlebacher, J. *J. Electrochem. Soc.* **2002**, *149*, B370-B377.

(65) Gómez-Marín, A. M.; Rizo, R.; Feliu, J. M. *Beilstein J. Nanotechnol.* **2013**, *4*, 956-967.

(66) Gong, K.; Choi, Y.; Vukmirovic, M. B.; Liu, P.; Ma, C.; Su, D.; Adzic, R. R. *Z. Phys. Chem.***2012**, *226*, 1025-1038.

(67) Greeley, J.; Stephens, I. E. L.; Bondarenko, A. S.; Johansson, T. P.; Hansen, H. A.; Jaramillo, T. F.; RossmeislJ; ChorkendorffI; Nørskov, J. K. *Nat. Chem.* **2009**, *1*, 552-556.

(68) Rossmeisl, J.; Logadottir, A.; Nørskov, J. K. *Chem. Phys.* **2005**, *319*, 178-184.

(69) Jinnouchi, R.; Kodama, K.; Hatanaka, T.; Morimoto, Y. *Phys. Chem. Chem. Phys.* **2011**, *13*, 21070-21083.

(70) Wang, G. X.; Wu, H. M.; Wexler, D.; Liu, H. K.; Savadogo, O. *J. Alloys Compd.* **2010**, *503*, L1-L4.

(71) Zhang, X.; Lu, G. *J. Phys. Chem. Lett.* **2014**, *5*, 292-297.

(72) Hammer, B.; Nørskov, J. K. *Adv. Catal.* **2000**, *45*, 71.

(73) Hofmann, T.; Yu, T. H.; Folse, M.; Weinhardt, L.; Bär, M.; Zhang, Y.; Merinov, B. V.; Myers, D. J.; Goddard, W. A.; Heske, C. *J. Phys. Chem. C* **2012**, *116*, 24016-24026.

(74) Mamatkulov, M.; Filhol, J. S. *Phys. Chem. Chem. Phys.* **2011**, *13*, 7675-7684.

(75) Wang, X.; Choi, S.-I.; Roling, L. T.; Luo, M.; Ma, C.; Zhang, L.; Chi, M.; Liu, J.; Xie, Z.; Herron, J. A.; Mavrikakis, M.; Xia, Y. *Nat. Commun.* **2015**, *6*.

(76) Sha, Y.; Yu, T. H.; Merinov, B. V.; Shirvanian, P.; Goddard, W. A. *J. Phys. Chem. Lett.* **2011**, *2*, 572-576.

(77) Yancey, D. F.; Zhang, L.; Crooks, R. M.; Henkelman, G. *Chem. Sci.* **2012**, *3*, 1033-1040.

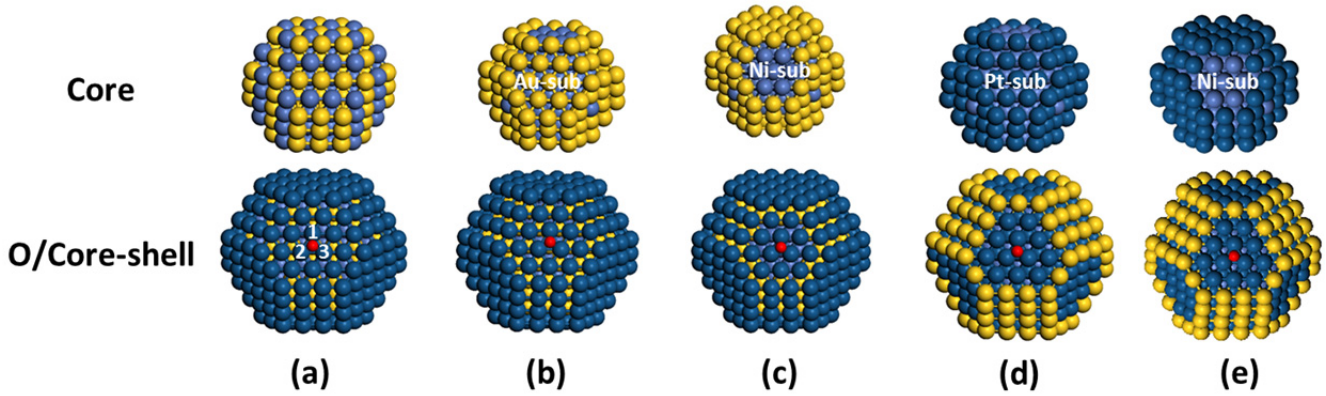

Figure 1. Pt(111) shells from three optimized core-shell NP models with the same composition. (a) $Ni_{96}Au_{105}@Pt_{204}$; (b) $Ni_{79}@Ni_{17}Au_{105}@Pt_{204}$, where the oxygen was adsorbed on the Pt(111) shell supported by Au IL; (c) $Ni_{79}@Ni_{17}Au_{105}@Pt_{204}$, where the oxygen was adsorbed on the Pt(111) shell supported by Ni IL; (d) $Ni_{79}@Ni_{17}Pt_{105}@Au_{105}Pt_{99}$, where the oxygen was adsorbed on the Pt(111) shell supported by Pt IL; (e) $Ni_{79}@Ni_{17}Pt_{105}@Au_{105}Pt_{99}$, where the oxygen was adsorbed on the Pt(111) shell supported by Ni IL. Light blue: Ni; dark blue: Pt, yellow: Au; red: O.

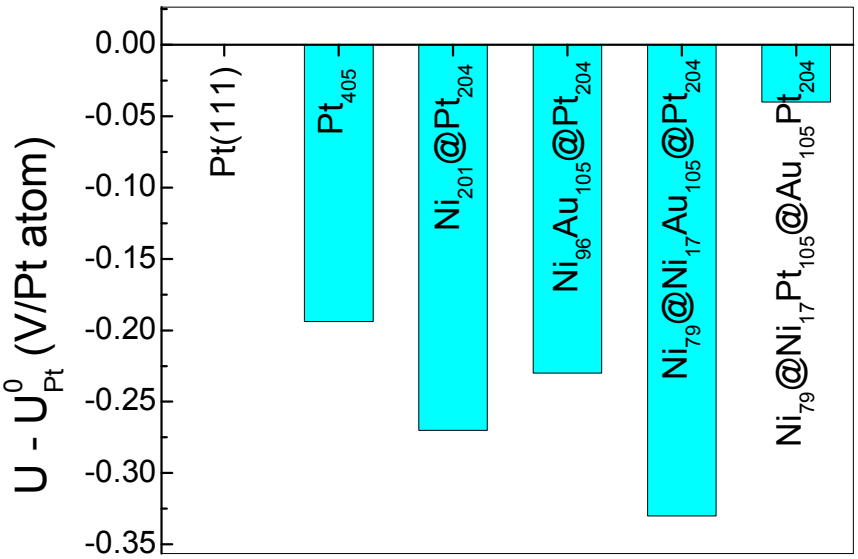

Figure 2. Calculated dissolution potentials for Pt, Ni@Pt and NiAu@ Pt NPs with respect to Pt(111).

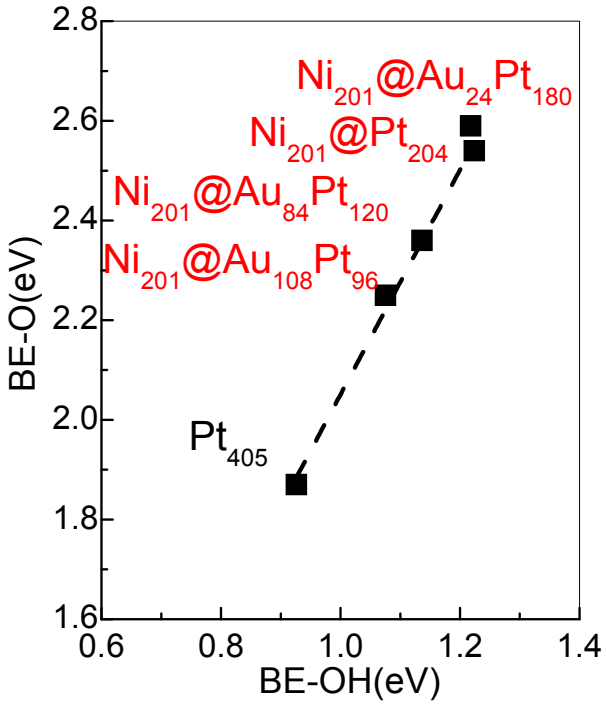

Figure 3. Calculated O-binding energy (BE-O) as a function of calculated OH-binding energy (BE-OH) on Pt(111) facet of Ni@Pt core-shell NPs.

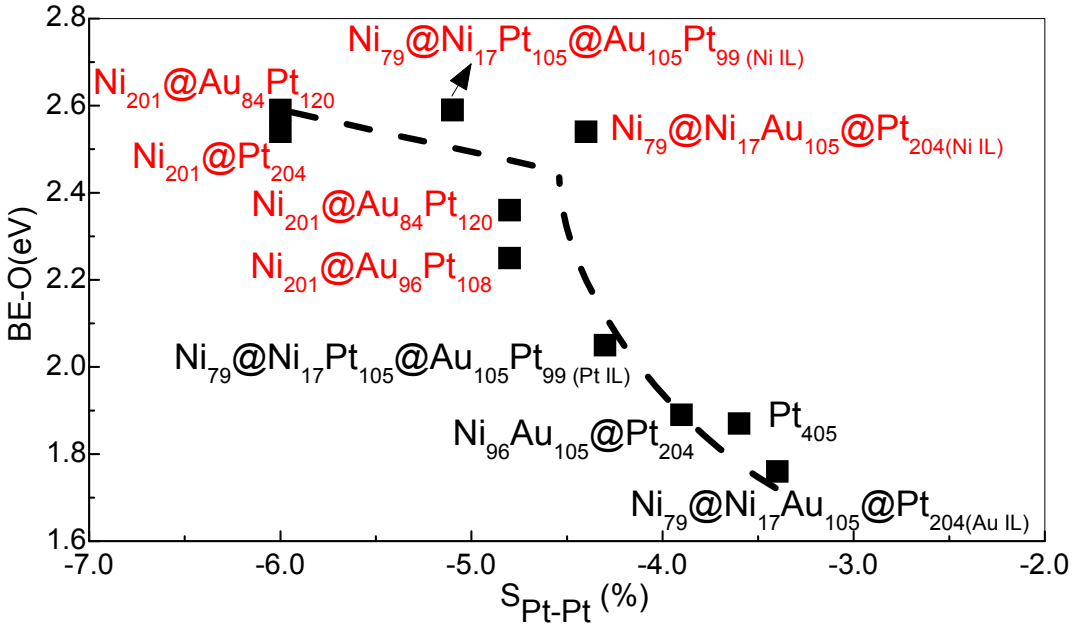

Figure 4. Variation of calculated O-binding energy (BE-O) with the strain ($S_{Pt\text{-}Pt}$) on the Pt(111) shell of core-shell NPs.

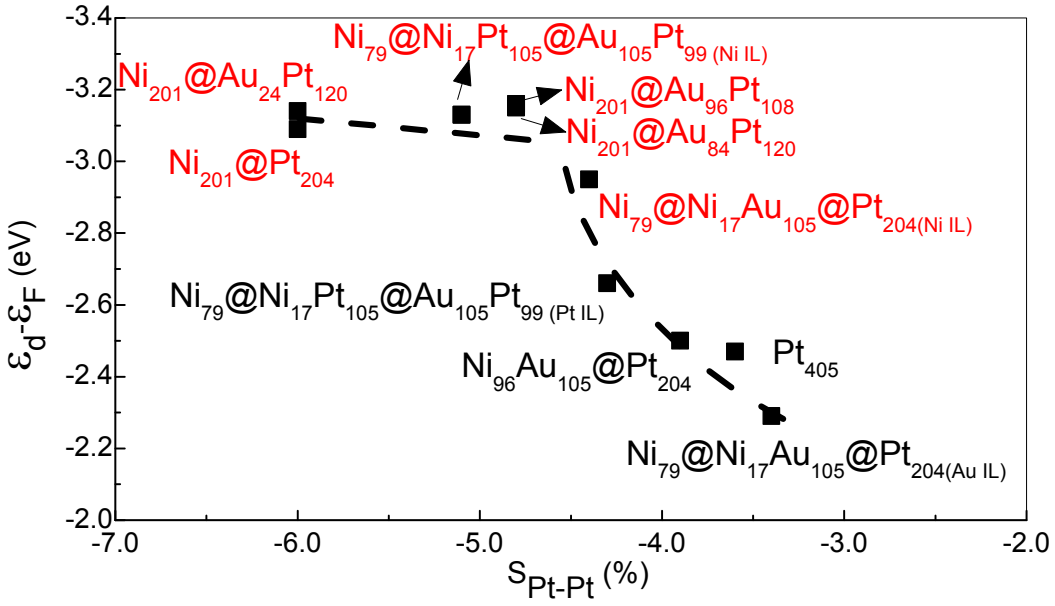

Figure 5. Calculated d-band center of three Pt atoms interacted with oxygen as a function of surface contraction.

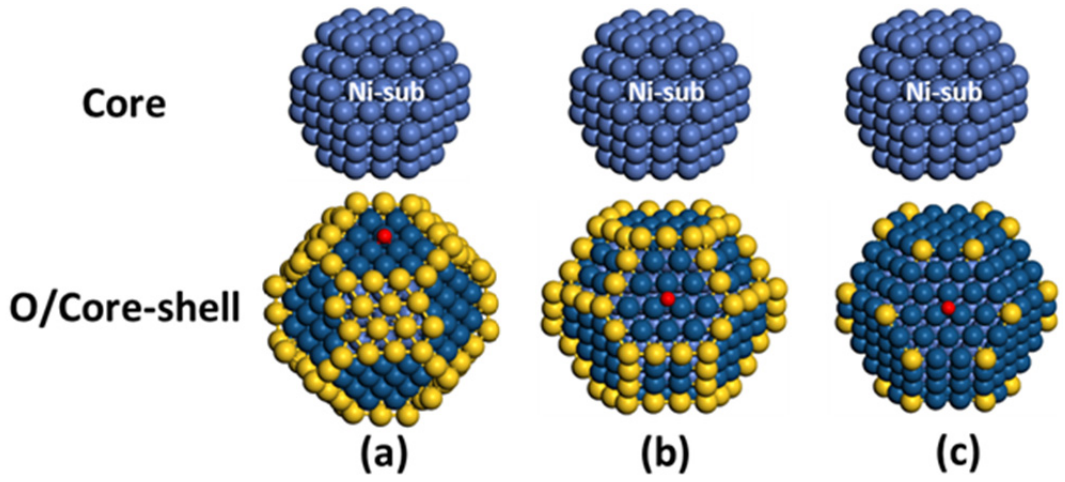

Figure 6. Optimized structures of three designed core-shell NP models. (a) $Ni_{201}@Au_{108}Pt_{96}$; (b) $Ni_{201}@Au_{84}Pt_{120}$; (c) $Ni_{201}@Au_{24}Pt_{180}$.

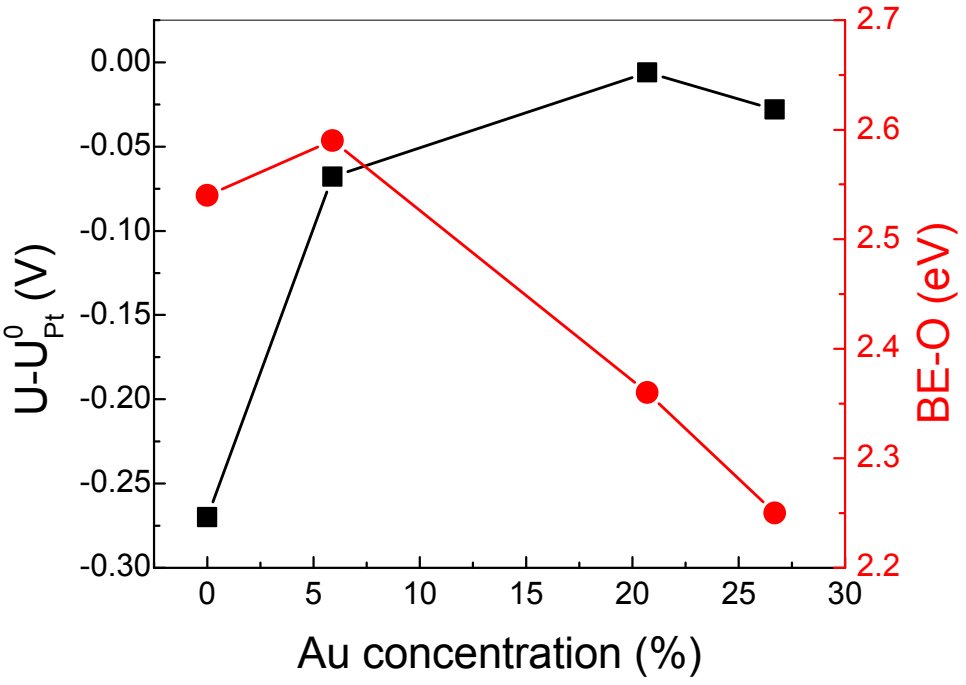

Figure 7. (a) Calculated dissolution potentials (U, black square) and O-binding energy (BE-O, red circle) as a function of Au concentration for Ni@AuPt core-shell nanoparticle.

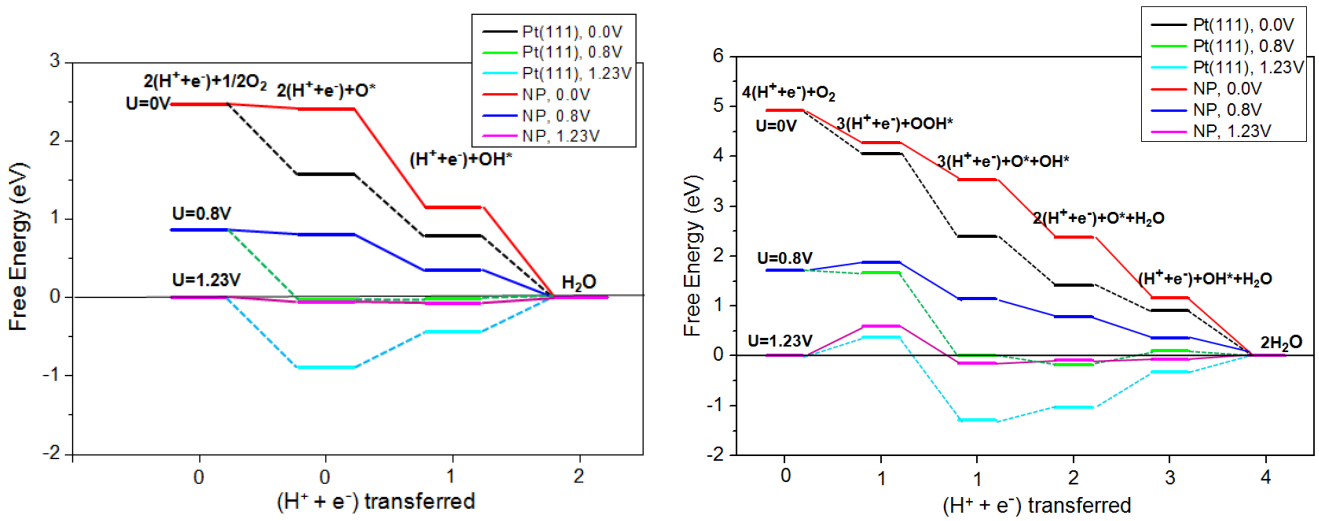

(a) (b)

Figure 8. Calculated free-energy diagram for the ORR over Pt(111) (dashed line) and Ni_{201}@($Au_{84}Pt_{120}$) NP (solid line) at zero potential (U=0V), the working electrode potential (U=0.8V), and the equilibrium potential (U=1.23 V), following (a) dissociative (direct) mechanism, and (b) associative (indirect) mechanism.

TOC

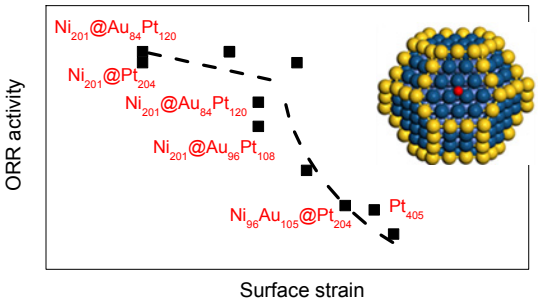
$Ni_{201}@Au_{84}Pt_{120}$
$Ni_{201}@Pt_{204}$
$Ni_{201}@Au_{84}Pt_{120}$
$Ni_{201}@Au_{96}Pt_{108}$
$Ni_{96}Au_{105}@Pt_{204}$
Pt_{405}
ORR activity
Surface strain